Research Article / *Araştırma Makalesi*

Ege Journal of Medicine / *Ege Tıp Dergisi* 2026; 65 (1): 107-113

Prostate gland segmentation on prostate magnetic resonance images: An artificial intelligence study using a U-net-based convolutional neural network

Prostat manyetik rezonans görüntülerinde prostat bezi segmentasyonu: U-net tabanlı sinir ağı kullanan bir yapay zeka çalışması

Başak Ünverdi[1] Mehmet Akif Özdemir[2] Aytuğ Onan[2] Elif Aylin Yüce Yörük[3] Türker Acar[1]

[1]Department of Radiology, University of Health Sciences Izmir Bozyaka Education and Research Hospital, Izmir/Türkiye

[2]Department of Biomedical Engineering, Faculty of Engineering and Architecture, Izmir Katip Çelebi University, Izmir/Türkiye

[3]Ministry of Health, Provincial Health Directorate, Muğla/Türkiye

ABSTRACT

Aim: The aim of this study is to automatically segment the prostate gland, transitional zone (TZ) and periferal zone (PZ) on prostate Magnetic Resonance Imaging (MRI) using a U-net based convolutional neural network (CNN).

Materials and Methods: This retrospective study included a total of 100 patients who underwent screening with a 1.5T MRI device between January and December 2020. The acquired images were evaluated by a senior radiology resident and converted to nifti format using the MedSeg.ai platform. Prostate and TZ masks were manually traced, while the remaining area (PZ) was automatically segmented by extracting the TZ mask from the prostate mask. A U-net based CNN algorithm with 7 depth layers was developed. Data from 80 patients were used for training the algorithm, with 10 randomly selected for validation. The remaining data from 20 patients were used for testing. Evaluation metrics applied on the test set included accuracy, mean and median Dice Similarity Coefficient (DSC), mean Hausdorff Distance (HSD), Mean Surface Distance (MSD), mean Relative Absolute Volume (RAV).

Results: Mean DSC of 0.91 ± 0.03, 0.87 ± 0.06, 0.70 ± 0.16 and median DSC of 0.92, 0.90, 0.75 were obtained for prostate gland, TZ and PZ segmentation respectively. Mean HSD was 8.58, 9.52, 18.78, MSD was 0.92, 0.84, 1.30 and mean RAV was 3.51, 9.87, 70.57 for the segmentation of aforementioned structures.

Conclusion: The developed U-net algorithm performed better in segmenting the prostate and TZ than in previous studies. While the success rate of PZ segmentation was lower, this could be attributed to various factors, as indicated by state-of-the-art methods in deep learning. This study highlights AI's promising role in automating prostate segmentation.

Keywords: MpMRI, CGI, CNN, U-net, artificial intelligence, deep learning.

ÖZ

Amaç: *Bu çalışmanın amacı, prostat Manyetik Rezonans Görüntüleme (MRG) cihazında prostat bezini, geçiş bölgesini (TZ) ve periferik bölgeyi (PZ) U-net tabanlı bir evrişimsel sinir ağı (CNN) kullanarak otomatik olarak segmentlere ayırmaktır.*

Corresponding author: Elif Aylin Yüce Yörük
Ministry of Health, Provincial Health Directorate, Muğla/Türkiye
E-mail:*elfaylinyuce@hotmail.com*
Application date: 01.08.2025 Accepted: 04.12.2025

Gereç ve Yöntem: *Bu retrospektif çalışmaya, Ocak ve Aralık 2020 tarihleri arasında 1,5T MR cihazıyla taramadan geçen toplam 100 hasta dahil edilmiştir. Elde edilen görüntüler, kıdemli bir radyoloji asistanı tarafından değerlendirilmiş ve MedSeg.ai platformu kullanılarak nifti formatına dönüştürülmüştür. Prostat ve TZ maskeleri manuel olarak izlenirken, kalan alan (PZ), prostat maskesinden TZ maskesi çıkarılarak otomatik olarak segmentlere ayrılmıştır. 7 derinlik katmanına sahip U-net tabanlı bir CNN algoritması geliştirilmiştir. Algoritmanın eğitimi için 80 hastadan alınan veriler kullanılmış ve 10 hasta doğrulama için rastgele seçilmiştir. Kalan 20 hastadan alınan veriler ise test için kullanılmıştır. Test setine uygulanan değerlendirme metrikleri arasında doğruluk, ortalama ve ortanca Dice Benzerlik Katsayısı (DSC), ortalama Hausdorff Mesafesi (HSD), Ortalama Yüzey Mesafesi (MSD) ve ortalama Bağıl Mutlak Hacim (RAV) yer aldı.*

Bulgular: *Prostat bezi, TZ ve PZ segmentasyonu için sırasıyla 0,91 ± 0,03, 0,87 ± 0,06, 0,70 ± 0,16 ortalama DSC ve 0,92, 0,90, 0,75 ortanca DSC elde edildi. Söz konusu yapıların segmentasyonu için ortalama HSD 8,58, 9,52, 18,78, MSD 0,92, 0,84, 1,30 ve ortalama RAV 3,51, 9,87 ve 70,57 olarak bulundu.*

Sonuç: *Geliştirilen U-net algoritması, prostat ve TZ segmentasyonunda önceki çalışmalara göre daha iyi performans göstermiştir. PZ segmentasyonunun başarı oranı daha düşük olsa da, bu durum derin öğrenmedeki en son yöntemlerin de gösterdiği gibi çeşitli faktörlere bağlanabilir. Bu çalışma, yapay zekanın prostat segmentasyonunun otomasyonunda oynadığı hayati rolü vurgulamaktadır.*

Anahtar Sözcükler: *MpMRI, CGI, CNN, U-net, yapay zeka, derin öğrenme*

INTRODUCTION

Prostate cancer accounts for 27% of all diagnosed cases, ranking as the second most common cause of cancer-related mortality among males (1). Early and accurate diagnosis is of the utmost importance to reduce mortality. The primary method for diagnosing prostate cancer is transrectal ultrasound-assisted biopsy (TRUS-Bx) (2).

In the 1980s, the introduction of magnetic resonance imaging (MRI) of the prostate allowed radiologists to locate, diagnose and stage lesions more accurately (3). In its original form, the MRI technique comprised solely T1- and T2-weighted sequences, which were employed for the purpose of anatomically evaluating the prostate gland and its constituent zones. However, in the current clinical practice, the addition of diffusion-weighted imaging (DWI) and dynamic contrast-enhanced (DCE) imaging allows the acquisition of functional details. Consequently, the current multiparametric prostate MRI (MpMRI) protocol is being employed not only for diagnostic purposes but also for active surveillance and the monitoring of treatment outcomes in patients. (4,5).

The increased use of MpMRI has also introduced alternatives to TRUS-bx. MRI-guided biopsies (MRGB) can be performed either in an MRI scanner (in-bore) or with TRUS guidance, which requires the integration of MRI with ultrasound imaging (6). The latter is only possible with the help of computer-based software that superimposes selected structural results compared to TRUS-bx and has a sensitivity of around 91% for diagnosing prostate cancer (7–9).

Segmentation of the prostate, transitional zone (TZ) and peripheral zone (PZ) on MRI is important for accurate categorisation of prostate lesions according to the Prostate Imaging-Reporting and Data System (PIRADS). It is also essential for improving the accuracy of MRI-TRUS fusion biopsies. In addition, prostate segmentation plays a key role in radiotherapy preparation and volume estimation of the gland to track prostate cancer progression (10,11). The automation of prostate segmentation using artificial intelligence (AI) algorithms has the potential to accelerate the aforementioned processes.

Convolutional neural networks (CNNs) are composed of artificial neurons that perform deep learning and are currently undergoing rigorous testing in the domain of prostate segmentation (12,13). The U-Net is a CNN that is fully automated and capable of identifying specified structures within the input data. It has demonstrated promising results for rapid and accurate segmentation (14).

The objective of this study is to develop an automated method for segmenting the prostate gland, transitional zone (TZ), and peripheral zone (PZ) on prostate magnetic resonance imaging (MRI) scans. Axial T2-weighted images were

selected for this purpose, as they provide the optimal anatomical detail. A U-net based seven-layer depth CNN was employed as a diagnostic tool to ascertain the location of prostate lesions and to direct targeted biopsies. This approach allows for the rapid and precise determination of potential lesion location, thereby facilitating the accurate assignment of PIRADS scores.

MATERIALS and METHODS

Retrospective analysis of all patients between 01/01/2020 and 01/01/2021 who underwent prostate multiparametric magnetic resonance imaging (MpMRI) at one large, urban teaching hospital were included. Patients whose image quality was inadequate for evaluation, whose images could not be transferred to the SYNGO.VIA workstation, or whose masking could not be performed due to technical limitations were excluded. The MRI studies for the imaging, included 100 patients were segmented by a senior radiology resident.

Using a 1.5T (Siemens Magnetom Aera, Siemens Healthcare, Erlangen, Germany) outlined in PIRADSv2.1 (15). Prior to undergoing an MRI scan, each patient is required to sign a consent form, which is typically obtained by the responsible technician. The purpose of the form is to ascertain whether any metallic prostheses, pacemakers, or other such devices may pose a risk or create artefacts during the MRI examination. Moreover, the form requests details regarding the patient's any previous surgical procedures. Magnetic resonance imaging (MRI) examinations are not performed on patients who are at risk. Furthermore, in patients with a history of allergic reactions to contrast agents, the examination is either cancelled or obtained without contrast. In patients who do not present contraindications, MRI examinations are considered to be safe and do not necessitate the implementation of additional safety precautions. Moreover, the consent form requests consent for the utilisation of images for any academic purposes. Ethical approval was granted by hospital ethics committee.

T2-weighted axial 3mm slices, were converted to the .nifti format using the MedSeg.ai platform. The prostate whole gland (WG) and transition zone (TZ) masks were delineated manually. The remaining areas were automatically segmented by subtracting the TZ masks from the prostate WG masks, subsequently obtaining the PZ masks (Figure-1).

The U-net had a seven-layer depth (Figure-2). The input images were resized from 320x320 to 256x256 using OpenCV's nearest interpolation technique. The encoding and decoding pathways employed convolution of 3x3, batch normalisation with the ReLU function and maxpooling of 2x2. The author(s) reviewed and edited the content, assuming full responsibility for the publication's content.

Python 3.7, Keras library with TensorFlow 2.8 infrastructure, CUDA 11.2 ve cuDNN 8 were used in developing training parameters. Ending the 100 patients were used in training the algorithm. Ten of these 80 were randomly selected for validation. The remaining 20 patients were used for the testing process. The algorithm was completely blind to the test data and none of the testing images were used in training.

The evaluation metrics were as follows: accuracy, mean and median Dice Similarity Coefficient (DSC), mean Hausdorff Distance (HSD), Mean Surface Distance (MSD), and mean Relative Absolute Volume (RAV).

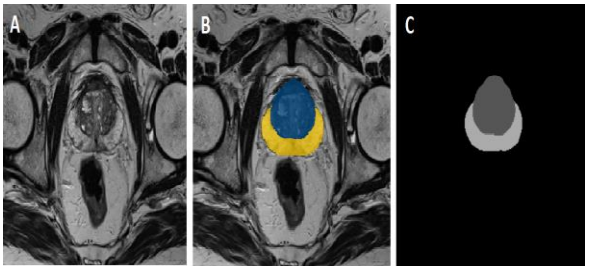

Figure-1. Prostate gland segmentation. (A) Source image, (B) Manual segmentation, (C) TZ and PZ masks

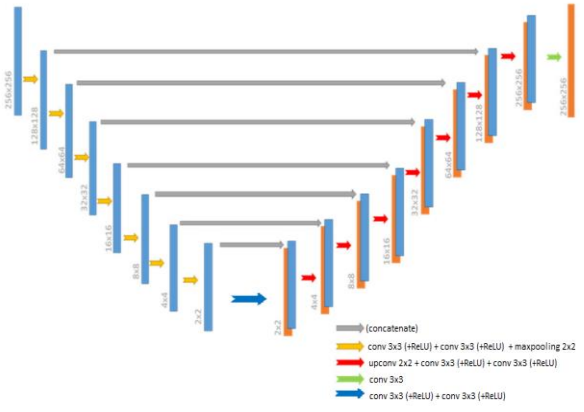

Figure-2. U-net based seven-layer depth CNN

RESULTS

Mean DSC of 0.91±0,03, 0.87±0,06, 0.70±0.16 and median DSC of 0.92, 0.90, 0.75 were obtained for prostate WG, TZ and PZ segmentation respectively. Mean HSD was 8.58, 9.52, 18.78, MSD was 0.92, 0.84, 1.30 and mean RAV was 3.51, 9.87, 70.57 for the segmentation of aforementioned structures (Table-1). The ground truth is indicated by red annotations, while the algorithmic predictions are represented in blue (Figure-3,4,5).

Table-1. Results for prostate WG, TZ and PZ segmentation

	ACCURACY	MEAN ± SD DSC	MEDIAN DSC	MEAN HSD	MSD	MEAN RAV
WG	0.936	0.913±0,03	0.929	8.587	0.928	3.511
TZ	0.919	0.879±0,06	0.902	9.521	0.848	9.876
PZ	0.746	0.706±0.16	0.758	18.784	1.302	70.577

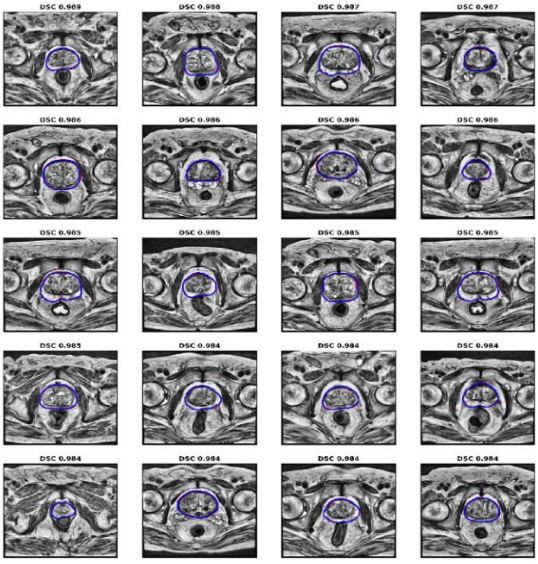

Figure-3. Best predictions for prostate WG segmentation

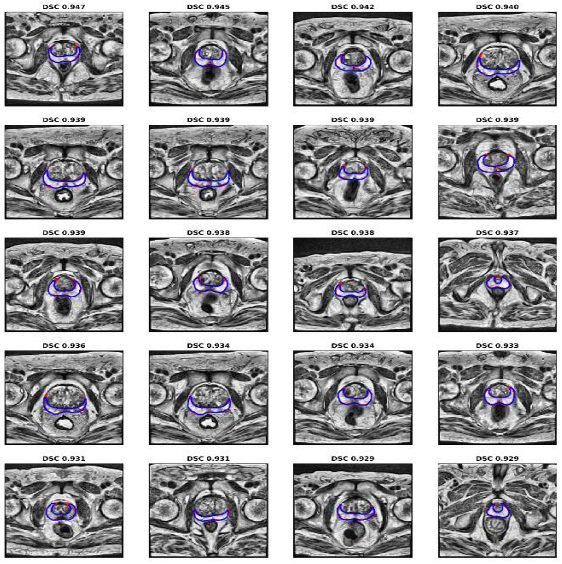

Figure-5. Best predictions for PZ segmentatio

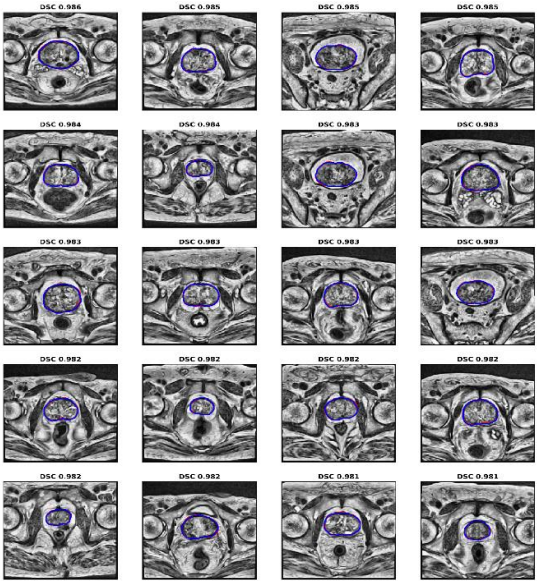

Figure-4. Best predictions for TZ segmentation

DISCUSSION

U-net based algorithms operate in a manner analogous to that of radiologists in the assessment of images. In the initial stage, the algorithm scans each image to ascertain the presence of the structure to be segmented. As the prostate gland is not present in every slice of the prostate MRI, the fully automated approach of the algorithm employed in this study obviates the necessity to select slices containing the gland. This feature facilitates the implementation of the algorithm in clinical practice, thereby assisting radiologists. The algorithm demonstrates an accuracy of 0.93 in defining the prostate gland in images. In the event that the prostate gland is not pre-defined within the image, a false negative segmentation of the gland will result in DSC values of 0 when compared to the ground truth. In a comparable study employing a U-net-based

algorithm, it was demonstrated that accurate identification of the gland enhances the DSC score by 3% (16).

Magnetic resonance imaging (MRI) scans are obtained in three distinct planes, thereby providing volumetric information. Three-dimensional segmentation (3D) models have been developed for use with this volumetric data, with the objective of mirroring the methodology employed by radiologists when reviewing all slices and evaluating them comprehensively (17–19). Nevertheless, the processing of this considerable quantity of data necessitates a greater investment of time, while the costs associated with computer systems are also on the rise. In this study, the U-net model is applied to 2D images, which can be assessed with greater ease and speed, thereby rendering it more suitable for routine clinical practice.

Two-dimensional systems have been integrated into three-dimensional models. The 3D input data is evaluated, and segmentation is conducted on the 2D output data, thereby facilitating comparisons with other 2D models. A hybrid model developed by Ushinsky et al. (20), yielded a mean DSC of 0.89 and a median DSC of 0.91, which is comperable to the current data.

In a study conducted by Jensen et al. (21), both 1.5T and 3T MRI data were employed to provide greater diversity. The mean DSC values for TZ and PZ segmentation were 0.808 (±0.102) and 0.694 (±0.183) for 1.5T images and 0.778 (±0.180) and 0.690 (±0.148) for 3T images, respectively. The model yielded superior results, with a mean DSC of 0.879 (±0.063) and 0.706 (±0.162), respectively. Nevertheless, our model has yet to be tested on 3T MRI data, and further evaluation is necessary.

CNN algorithms can be applied to other sequences in mpMRIs. Zabihollahy et al. (22) employed both T2-weighted imaging (T2-WI) and diffusion-weighted imaging (DWI) for segmenting the transitional zone (TZ), and peripheral zone (PZ). The resulting median DSC values for T2-WI were 0.95, 0.93, and 0.86, respectively with the improvement likely reflecting the additional data included in this project.

PZ segmentation presents two principal challenges. First, a volume of interest is small, even a minor error results in a significant decline in DSC values. Second, the differentiation of PZ from periprostatic fat represents a significant challenge, even for radiologists. Consequently, a considerable number of existing models described in the literature have yielded less favourable PZ segmentation when compared to the current study (23–25).

One limitation of this study is that the algoritm was tested only to 20 images. To be candid, when selecting an MRI, the only specification provided was a date range. The decision was taken not to utilise any additional criteria with the objective of facilitating the training of the algorithm on as many patients as possible, irrespective of their cancer status. This approach was adopted to ensure the algorithm's capacity for accurate segmentation in complex cases.

The performance of the algorithm was found to be significantly compromised in patients who had previously undergone transurethral resection of the prostate (TURP). Typical MRI appearances include a central, funneled resection cavity that is contiguous with the bladder neck. The size and shape of this cavity vary depending on the volume of transition zone resected. These alterations disrupt the expected glandular morphology utilised by AI models for boundary recognition. The resection cavity is frequently incorporated within the segmented prostate, resulting in the extension of the contour into the urethral tract. Depending on the size of the cavity and the characteristics of the signal, the algorithm has either over-segmented the residual tissue or under-segmented the central gland. In the event of the cavity containing urine, or displaying irregular scarring, the signal intensity is subject to further disruption, thereby engendering confusion within the algorithm. It is evident that the modified post-surgical configuration constitutes a high-risk failure mode for automated segmentation, often necessitating manual correction.

The natural anatomic continuity at the prostate base, in conjunction with partial-volume effects, renders it challenging for the algorithm to accurately distinguish the capsule–seminal vesicle interface. Consequently, this may result in the erroneous inclusion of part or all of the seminal vesicles within the prostate contour, particularly when their T2 signal intensity is similar to that of the adjacent transition zone. The inclusion of such elements gives rise to an irregular, lobulated contour, which does not accurately reflect the prostatic outline. This, in turn, complicates downstream tasks such as lesion detection, staging, and treatment planning.

The utilisation of a compatible interface has the potential to address the challenges associated with PACS integration and the technical constraints of such applications in clinical practice.

CONCLUSION

The U-net-based seven-layer depth algorithm applied to 2D T2-weighted images yielded PZ segmentation results that were comparable to those of many current studies. The results obtained from this study are informative with regard to the current state of art deep learning methods, and they demonstrate the potential for future automated and semi-automated strategies that have the capacity to reduce the workload of radiologists for targeted prostate cancer patients.

Conflict of Interest: The authors declare that they have no conflict of interest.

Acknowledgements: None.

References

1. Siegel RL, Miller KD, Fuchs HE, Jemal A. Cancer statistics, 2022. CA Cancer J Clin. 2022 Jan;72(1):7–33.
2. Das CJ, Razik A, Sharma S, Verma S. Prostate biopsy: when and how to perform. Clin Radiol. 2019 Nov 1;74(11):853–64.
3. Yacoub JH, Oto A, Miller FH. MR Imaging of the prostate. Radiol Clin North Am. 2014;52(4):811–37.
4. Hoeks CMA, Barentsz JO, Hambrock T, Yakar D, Somford DM, Heijmink SWTPJ, et al. Prostate cancer: Multiparametric MR imaging for detection, localization, and staging. Radiology. 2011;261(1):46–66.
5. Durmus T, Baur A, Hamm B. Multiparametric magnetic resonance imaging in the detection of prostate cancer. Aktuelle Urol. 2014 Mar;45(2):119–26.
6. Drost FJH, Osses DF, Nieboer D, Steyerberg EW, Bangma CH, Roobol MJ, et al. Prostate MRI, with or without MRI-targeted biopsy, and systematic biopsy for detecting prostate cancer. Cochrane Database of Systematic Reviews. 2019;
7. Schoots IG, Roobol MJ, Nieboer D, Bangma CH, Steyerberg EW, Hunink MGM. Magnetic resonance imaging-targeted biopsy may enhance the diagnostic accuracy of significant prostate cancer detection compared to standard transrectal ultrasound-guided biopsy: a systematic review and meta-analysis. Eur Urol. 2015 Sep 1;68(3):438–50.
8. Kasivisvanathan V, Rannikko AS, Borghi M, Panebianco V, Mynderse LA, Vaarala MH, et al. MRI-Targeted or Standard Biopsy for Prostate-Cancer Diagnosis. N Engl J Med. 2018 Mar 18;378(19).
9. Fiard G, Hohn N, Descotes JL, Rambeaud JJ, Troccaz J, Long JA. Targeted MRI-guided prostate biopsies for the detection of prostate cancer: Initial clinical experience with real-time 3-dimensional transrectal ultrasound guidance and magnetic resonance/transrectal ultrasound image fusion. Urology. 2013 Jun 1;81(6):1372–8.
10. Pasquier D, Lacornerie T, Vermandel M, Rousseau J, Lartigau E, Betrouni N. Automatic segmentation of pelvic structures from magnetic resonance images for prostate cancer radiotherapy. Int J Radiat Oncol Biol Phys. 2007 Jun 1;68(2):592–600.
11. Toth R, Bloch BN, Genega EM, Rofsky NM, Lenkinski RE, Rosen MA, et al. Accurate prostate volume estimation using multifeature active shape models on T2-weighted MRI. Acad Radiol. 2011 Jun;18(6):745–54.
12. Zhu Y, Wei R, Gao G, Ding L, Zhang X, Wang X, et al. Fully automatic segmentation on prostate MR images based on cascaded fully convolution network. J Magn Reson Imaging. 2019 Apr 1;49(4):1149–56.
13. To MNN, Vu DQ, Turkbey B, Choyke PL, Kwak JT. Deep convolutional neural network for prostate MR segmentation. Int J Comput Assist Radiol Surg. 2018 Nov 1;13(11):1687.
14. Ronneberger O, Fischer P, Brox T. U-Net: Convolutional Networks for Biomedical Image Segmentation. Lecture Notes in Computer Science (including subseries Lecture Notes in Artificial Intelligence and Lecture Notes in Bioinformatics). 2015;9351:234–41.
15. Scott R, Misser SK, Cioni D, Neri E. PI-RADS v2.1: What has changed and how to report. SA J Radiol. 2021;25(1):1–13.
16. Clark T, Zhang J, Baig S, Wong A, Haider MA, Khalvati F. Fully automated segmentation of prostate whole gland and transition zone in diffusion-weighted MRI using convolutional neural networks. J Med Imaging (Bellingham). 2017 Oct 17;4(4):1.

17. Çiçek Ö, Abdulkadir A, Lienkamp SS, Brox T, Ronneberger O. 3D U-net: Learning dense volumetric segmentation from sparse annotation. Lecture Notes in Computer Science (including subseries Lecture Notes in Artificial Intelligence and Lecture Notes in Bioinformatics). 2016;9901 LNCS:424–32.
18. Yu L, Yang X, Chen H, Qin J, on PHT first A conference, 2017 undefined. Volumetric ConvNets with mixed residual connections for automated prostate segmentation from 3D MR images. aaai.org.
19. Milletari F, Navab N, Ahmadi SA. V-Net: Fully Convolutional Neural Networks for Volumetric Medical Image Segmentation. Proceedings - 2016 4th International Conference on 3D Vision, 3DV 2016. 2016 Jun 15;565–71.
20. Ushinsky A, Bardis M, Glavis-Bloom J, Uchio E, Chantaduly C, Nguyentat M, et al. A 3D-2D Hybrid U-Net Convolutional Neural Network Approach to Prostate Organ Segmentation of Multiparametric MRI. AJR Am J Roentgenol. 2021 Jan 1;216(1):111–6.
21. Jensen C, Sørensen KS, Jørgensen CK, Nielsen CW, Høy PC, Langkilde NC, et al. Prostate zonal segmentation in 1.5T and 3T T2W MRI using a convolutional neural network. J Med Imaging (Bellingham). 2019 Feb 22;6(1):1.
22. Zabihollahy F, Schieda N, Krishna Jeyaraj S, Ukwatta E. Automated segmentation of prostate zonal anatomy on T2-weighted (T2W) and apparent diffusion coefficient (ADC) map MR images using U-Nets. Med Phys. 2019 Jul 1;46(7):3078–90.
23. Aldoj N, Biavati F, Michallek F, Stober S, Dewey M. Automatic prostate and prostate zones segmentation of magnetic resonance images using DenseNet-like U-net. Scientific Reports 2020 10:1. 2020 Aug 31;10(1):1–17.
24. Litjens G, Toth R, van de Ven W, Hoeks C, Kerkstra S, van Ginneken B, et al. Evaluation of prostate segmentation algorithms for MRI: the PROMISE12 challenge. Med Image Anal. 2014 Feb;18(2):359.
25. Zabihollahy F, Ukwatta E, Krishna S, Schieda N. Fully automated localization of prostate peripheral zone tumors on apparent diffusion coefficient map MR images using an ensemble learning method. J Magn Reson Imaging. 2020 Apr 1;51(4):1223–34.